



High-Speed Interconnect Modeling and High-Accuracy Simulation Using SPICE and Finite Element Methods

Tai-Yu Chou, Jay Cosentino and Zoltan J. Cendes[†]

Ansoft Corporation, Pittsburgh, PA 15219

[†]Electrical and Computer Engineering Department
Carnegie Mellon University, Pittsburgh, PA 15213

Abstract

SPICE-based interconnection simulation is described for multiple coupled lines and for lines with three-dimensional discontinuities. Two- and three-dimensional finite element methods are presented for the quasi-TEM analysis of arbitrary interconnection structures. Partial capacitance and partial inductance values for three-dimensional discontinuities are obtained by defining input and output ports for the discontinuity and deembedding the two-dimensional regions to the plane of the discontinuity. This procedure is highly accurate and reliable and can be used to model arbitrary interconnect geometries. Interconnection circuits are entered via geometric CAD and are meshed and solved automatically by using adaptive mesh generation. Equivalent circuit models of typical 3D interconnects such as bends, vias, T junctions and chip packages are described. Simulations are based on modal decomposition for multiple lines implemented using SPICE. We show that the quasi-TEM analysis and the full wave analysis of a T-junction are nearly identical up to 10 GHz.

1 Introduction

The performance of high density, high speed digital system is limited today by the ability of digital interconnects to transmit signals undisturbed, undistorted and without excessive delay. Such delays and distortions are produced by underlying electromagnetic nature of electrical signals and produces transmission line effects such as reflection, dispersion, delay, and crosstalk. Simulation of these effects requires detailed three dimensional electromagnetic analysis. Yet, to date, electromagnetic interconnect simulation has been limited to simple two and three dimensional geometries. Many interconnection structures involve complicated shapes that are poorly approximated by existing simulation techniques. Further, two types of electromagnetic waves propagation exist in transmission lines. One type of wave propagation is quasi-TEM that is well modeled by using lumped L and C matrices and the method of characteristics. The other type of wave propagation requires full-wave analysis and best solved in terms of S-

parameters. It is not clear when quasi-TEM analysis is valid and when full-wave analysis is required.

This paper presents a new approach to interconnection simulation. The approach uses the finite element method to compute electromagnetic fields and allows any three-dimensional interconnection structure to be modeled accurately. It introduces a new definition and a new method of computing partial inductances and partial capacitances for three-dimensional interconnects. It examines the range of validity of the quasi-TEM approximation and demonstrates by using both full-wave and quasi-TEM analysis that quasi-TEM is accurate for a T-junction circuit up to 10 GHz. Finally, we show how to model multiple coupled lines correctly in SPICE even though SPICE directly supports only single conductor transmission lines.

A key component of this procedure is the application of deembedding to three-dimensional interconnect analysis. Deembedding allows partial capacitances and partial inductances to be defined without introducing the "overlap" between neighboring circuit elements produced by traditional methods. Previously, deembedding was only employed in high-frequency microwave circuit simulation with S-parameters [1]. The solution procedure in this paper is fully automated so that the physical description of the interconnection geometry can be entered by using existing CAD systems and solved with only minor additional input by the user.

2 Interconnection Electromagnetics

Wave propagation in an interconnect circuit is quasi-TEM if the delays resulting from 3D discontinuities are smaller than one tenth of the signal risetime [2]. This implies that if the size of discontinuities are small compared to the signal wavelength, retardation effects can be neglected. Two-dimensional traces may be any number of wavelength long and will of course exhibit retardation. However, as a rule of thumb, provided that three-dimensional discontinuities are less than one tenth of a wavelength long, it is possible to model the interconnection circuit as a set of coupled transmission lines with lumped elements used to represent the 3D discontinuities.

Consider a typical interconnect discontinuity such as the

30th ACM/IEEE Design Automation Conference[®]

Permission to copy without fee all or part of this material is granted provided that the copies are not made or distributed for direct commercial advantage, the ACM copyright notice and the title of the publication and its date appear, and notice is given that copying is by permission of the Association for Computing Machinery. To copy otherwise, or to republish, requires a fee and/or specific permission.

©1993 ACM 0-89791-577-1/93/0006-0684 1.50

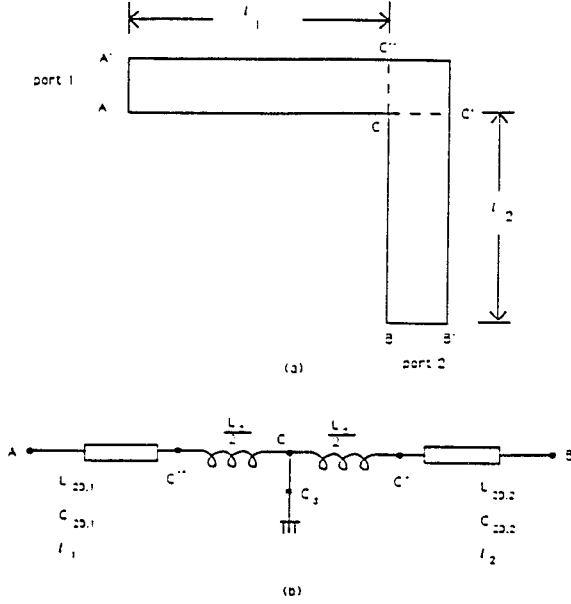


Figure 1: (a) The geometry of a right-angled bend. (b) Its equivalent circuit.

bend shown in Figure 1(a). To model this problem properly, we must determine the propagation characteristics of the input and output leads and the equivalent circuit of the 3D discontinuity. The propagation of a signal along the input and output leads are described by the telegrapher's equations while the discontinuity is described by lumped inductance and capacitance matrices. From an electromagnetic point of view, it is first required to solve the two 2D problems at the input and output ports and then to solve the 3D discontinuity.

2.1 Partial Capacitance

The key to computing partial capacitance is to express capacitance in terms of energy. For example, let ϕ_i be the solution of the Poisson equation

$$\nabla \cdot \epsilon \nabla \phi_i = -\rho \quad (1)$$

where one volt is applied to conductor i and all other conductors are grounded. It can be shown that the capacitance matrix of the system of conductors is given by [3]

$$C_{ij} = \int_{\Omega} \vec{E}_i \cdot \vec{D}_j d\Omega \quad (2)$$

where $\vec{E}_i = -\nabla \phi_i$ and $\vec{D}_i = \epsilon \vec{E}_i$ and Ω represents all space. Thus, the capacitance equals the integral of $\vec{E} \cdot \vec{D}$ over all space. To define a partial capacitance, therefore, we must find a way to partition space so that the integration in (2) is performed in each region separately without overlap.

Referring to the bend in Figure 1(a), we may define the capacitance per unit length of the port solutions as

$$C_{ij}^{2D_p} = \int_{\Omega_{2D_p}} \vec{E}_i \cdot \vec{D}_j d\Omega \quad (3)$$

where Ω_{2D_p} is the two-dimensional cross-section of port p . Let us define the capacitance of the 3D discontinuity region in Figure 1 as

$$C_{ij}^{3D} = \int_{\Omega_{3D}} \vec{E}_i \cdot \vec{D}_j d\Omega \quad (4)$$

We would like capacitance of a section of line containing the discontinuity to be given by

$$C_{ij} = C_{ij}^{3D} + \sum_{p=1}^N l_p C_{ij}^{2D_p} \quad (5)$$

where l_p is the length of the two-dimensional line outside the discontinuity region and N represents the number of ports.

In order for equation (5) to be exact, there can be no overlap between the 3D and the 2D regions. This condition is enforced by computing the 2D port boundaries.

2.2 Deembedding

Imposing the 2D port solutions as boundary conditions on the 3D discontinuity problem is accurate provided that the ports are not close to the discontinuity. However, the farther the ports are from the discontinuity, the longer the length of line included in the 3D region. This affects the quasi-TEM model, which assumes a uniform propagation delay along the 2D line. For this reason, it is important to extract the 3D discontinuity capacitance matrix by subtracting the 2D capacitance of the leads

$$C_{ij}^{dis} = C_{ij}^{3D} - \sum_{p=1}^N d_p C_{ij}^{2D_p} \quad (6)$$

where d_p is the deembedding distance at port p . Combining equations (5) and (6) gives

$$C_{ij} = C_{ij}^{dis} + \sum_{p=1}^N (l_p + d_p) C_{ij}^{2D_p} \quad (7)$$

Equation (7) is more exact than equation (5) for two reasons. First, the 2D capacitance matrices are in general more accurate than the 3D matrices since finer solutions are possible in 2D than in 3D. Second, propagation delays based on (7) take the full length of the 2D line into account instead of being shortened by distance from the discontinuity to the ports.

2.3 Partial Inductance

Many aspects of inductance calculations are similar to those of capacitance. We assume that all conductors and ground are perfect conductors so that skin effect is fully established. It follows that the current flows in thin sheets on the conductor surfaces and are distributed such that the magnetic field normal to the surface is zero. Fully developed skin effect is modeled by applying appropriate boundary conditions on the magnetic field.

The inductance matrix is computed from the field obtained by setting unit current to flow in one conductor and leaving all others open. Let \vec{H}_p be a particular solution of Ampere's law

$$\nabla \times \vec{H}_{pi} = \vec{J}_i \quad (8)$$

where the current density \vec{J}_i satisfies

$$\int_{\Omega_i} \vec{J}_i d\Omega = \delta_{ij} \quad (9)$$

where $\delta_{ij} = 1$ if $i = j$, $\delta_{ij} = 0$ otherwise. The total magnetic field satisfies

$$\vec{H}_i = \vec{H}_{pi} + \nabla \psi_i \quad (10)$$

The particular solution \vec{H}_p is computed locally by assigning tangential values of \vec{H}_p to satisfy Ampere's law. The homogeneous solution ψ_i satisfies the Poisson equation

$$\nabla \cdot \mu \nabla \psi_i = -\nabla \cdot \mu \vec{H}_{pi} \quad (11)$$

where μ is the permeability of the materials. The inductance matrix of a system of conductors is given by

$$L_{ij} = \int_{\Omega} \vec{B}_i \cdot \vec{H}_j d\Omega \quad (12)$$

where $\vec{B}_i = \mu \vec{H}_i$ is the magnetic flux density.

2.4 Finite Element Solution

The electromagnetic field problems in the preceding sections are solved by using finite element methods. The geometry of the interconnect structure is entered by using a solid modeling system. CAD translators for GDSII and DXF files are provided. After the problem geometry is entered, all the user needs to do is to specify the conductors in the system and to say "solve". The software automatically creates a finite element mesh, solves for the electric and magnetic fields, and adaptively refines the mesh until the L and C values are within a user specified tolerance.

The mesh generation procedure used in the software is Delaunay tessellation with adaptive mesh refinement[4]. The refinement criteria is based on an element by element residual calculation [5]. The software initially computes the 2D solution at the input and output ports, then sets these solutions as boundary conditions for the 3D problem. The final results from the software are the 2D and 3D L and C matrices for the structure as well as potentials and fields everywhere in the solution region. A variety of post-processing functions are available including a stack-oriented calculator by which any 2D and 3D quantity may be evaluated.

2.5 Examples

2.5.1 Right-Angled Bend

The above method is first illustrated for the case of a symmetrical right-angled bend. The top view of the bend is shown in Figure 1(a). It is assumed that the trace at ports 1 and 2 is semi-infinite.

To calculate the inductance of the bend, we first define two ports AA' and BB' as illustrated. The locations of these ports are arbitrary except that they must be far enough from the bend so that the field and current distributions differ negligibly from the straight line distributions. We also define reference planes CC' and DD' to define the deembedding distance l_1 and l_2 . The bend inductance L_d is given by the 3D inductance of the section between ports 1 and 2 minus the deductions for the deembedding lengths

$$L_d = L_{AB} - (l_1 L_{2D,1} + l_2 L_{2D,2}) \quad (13)$$

where $L_{2D,1}$ and $L_{2D,2}$ are the inductance per unit length of the conductors at ports 1 and 2. The bend capacitances are defined similarly.

The equivalent circuit for the bend is therefore given in terms of l_i , $L_{2D,i}$ and $C_{2D,i}$, L_d and C_d as shown in Figure 1(b).

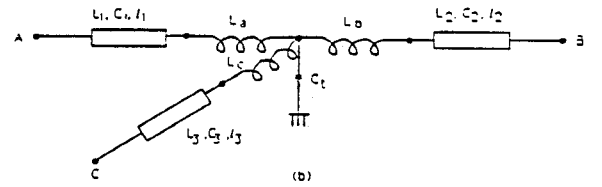
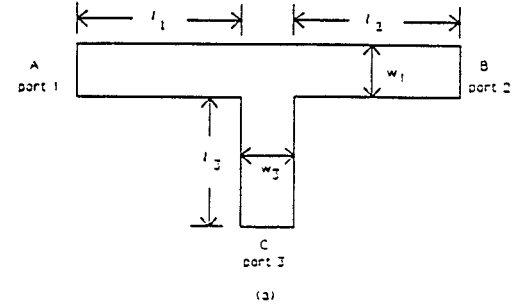


Figure 2: (a) The geometry of a T-junction. (b) Its equivalent circuit.

2.5.2 T-Junction

A general T-junction has the structure shown in Figure 2(a) where the traces may be of different widths w_1 and w_3 . The equivalent circuit for this structure is given in Figure 2(b). Since there are three different inductance values L_a , L_b and L_c , three equations are needed to determine these values. These equations are obtained by:

1. Injecting one ampere from A to C with B open.
2. Injecting one ampere from A to B with C open.
3. Injecting one ampere from C to B with A open.

This generates the following equations

$$L_{3D}^{AC} - L_{2D}^A l_1 - L_{2D}^C l_3 = L_{3D}^a + L_{3D}^c \quad (14)$$

$$L_{3D}^{AB} - L_{2D}^A l_1 - L_{2D}^B l_2 = L_{3D}^a + L_{3D}^b \quad (15)$$

$$L_{3D}^{CB} - L_{2D}^B l_2 - L_{2D}^C l_3 = L_{3D}^c + L_{3D}^b \quad (16)$$

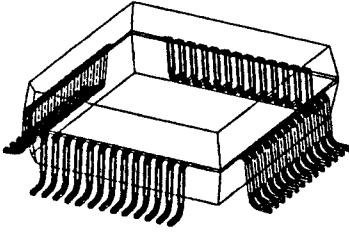


Figure 3: A 52 pins Quad Flat Pack.

2.5.3 Quad Flat Pack

A more complicated interconnect structure is provided by the 52 pin Quad Flat Pack (QFP) shown in Figure 3. Using symmetry, the L and C matrices of this structure may be computed by solving one quarter of the problem four times, applying Dirichlet and Neumann boundary conditions on the planes of symmetry, and averaging the results [3]. Since the resulting 13 by 13 L and C matrices consume a large space, only the matrix values for pins 41 to 44 are given here

$$C = \begin{bmatrix} 94.2 & -28.4 & -4.87 & -3.03 \\ -28.4 & 94.4 & -28.5 & -5.82 \\ -4.87 & -28.5 & 94.2 & -30.3 \\ -3.03 & -5.82 & -30.3 & 83.8 \end{bmatrix} fF$$

$$L = \begin{bmatrix} 2.75 & 1.15 & 0.85 & 0.68 \\ 1.15 & 2.70 & 1.15 & 0.87 \\ 0.85 & 1.15 & 2.61 & 1.22 \\ 0.68 & 0.87 & 1.22 & 3.07 \end{bmatrix} nH$$

3 Coupled Transmission Line and Lumped Element Models

As described in the preceding sections, quasi-TEM waves in interconnect structures may be modeled using multiconductor 2D transmission line theory and lumped elements to represent the 3D discontinuities. Coupled transmission lines are characterized by the 2D L and C matrices at the

ports while 3D discontinuities are represented by equivalent T networks.

The propagation of TEM waves along an n conductor plus ground transmission line is governed by the telegrapher's equations

$$\frac{\partial}{\partial x} \begin{bmatrix} V \\ I \end{bmatrix} = -\frac{\partial}{\partial t} \begin{bmatrix} 0 & L \\ C & 0 \end{bmatrix} \begin{bmatrix} V \\ I \end{bmatrix} \quad (16)$$

where V and I are vectors of length n and contain the line voltage and current. Signal propagation with quasi-TEM waves may be modeled via modal decomposition [6]. Using similarity transformations to diagonalize the matrix, equation (16) can be written in modal form

$$\frac{\partial}{\partial x} \begin{bmatrix} V_m \\ I_m \end{bmatrix} = -\frac{\partial}{\partial t} \begin{bmatrix} 0 & L_m \\ C_m & 0 \end{bmatrix} \begin{bmatrix} V_m \\ I_m \end{bmatrix} \quad (17)$$

with

$$\begin{bmatrix} V \\ I \end{bmatrix} = \begin{bmatrix} M_V & 0 \\ 0 & M_I \end{bmatrix} \begin{bmatrix} V_m \\ I_m \end{bmatrix} \quad (18)$$

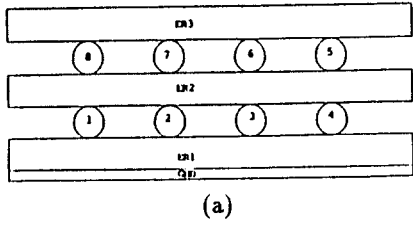
where V_m and I_m are modal voltage and current, and M_V and M_I are voltage and current eigenvectors. This decouples the n lines into n fundamental modes.

Modal decomposition decouples the telegrapher's equations into n fundamental modes. This allows us to bridge the gap between SPICE, which models only single conductor transmission lines, and the physics, which says that transmission lines in a multiconductor system are coupled. Modal decomposition converts multiple lines into an equivalent set of uncoupled lines for SPICE simulation. Thus, the range of application of SPICE is extended to include effects such as crosstalk, multiple delays, reflections and dispersion found on multiconductor lines. This means that the simulation is SPICE compatible and provides accurate voltage and current waveforms in the time domain.

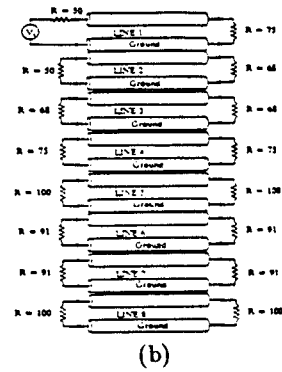
4 Examples and Results

4.1 An Eight-Conductor Line

An eight-conductor interconnect structure above ground is shown in Figure 4(a). The simulation for this structure is compared to measurements to determine its accuracy. The thickness of the dielectrics and the diameter of the conductors are both 187.5mil. The relative permittivity of the dielectric between the conductors is 2.25. Figure 4(b) shows the terminations of the conductors used in the measurements. Figure 5(a) shows the simulated and measured voltage waveforms at both the near and far ends of the active line #1. Figure 5(b) shows the simulated and measured voltage waveforms at the near and far ends of the passive line #2. The simulated waveforms are almost identical to the measured waveforms on every one of the eight lines and at every instant in time.

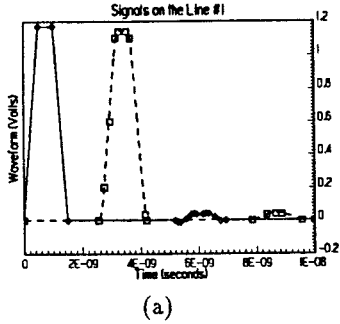


(a)

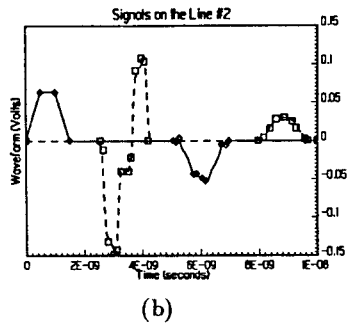


(b)

Figure 4: (a) An eight conductor transmission line. (b) The line terminations. Line #1 is the active line; all others are passive lines.

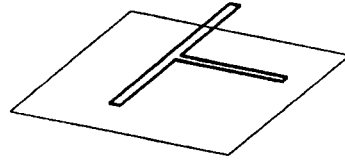


(a)

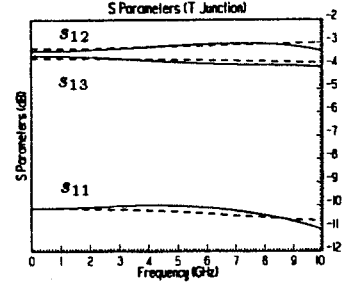


(b)

Figure 5: Simulated and measured voltage waveforms. (a) Solid and dashed lines are the simulated signals at near and far ends of line #1. ◇ and □ are the corresponding measured data. (b) Solid and dashed lines are the simulated signals at near and far ends of line #2. ◇ and □ the corresponding measured data.



(a)



(b)

Figure 6: (a) A T-junction above a ground plane. (b) S-parameter of the T-junction from full wave solution (solid line) and using quasi-TEM models with lumped elements (dashed line).

4.2 T-Junction

Figure 6(a) shows T-Junction circuit above a ground plane. The transmission line model parameters from finite element solution and deembedding are

$$L_{left}^{2d} = 5.28 \times 10^{-7} H/m$$

$$C_{left}^{2d} = 2.01 \times 10^{-11} F/m$$

$$L_{right}^{2d} = 5.28 \times 10^{-7} H/m$$

$$C_{right}^{2d} = 2.01 \times 10^{-11} F/m$$

$$L_{front}^{2d} = 5.84 \times 10^{-7} H/m$$

$$C_{front}^{2d} = 1.81 \times 10^{-11} F/m$$

$$C^{3d} = 5.9 \times 10^{-14} F$$

$$L_{left}^{3d} = 3.5 \times 10^{-10} H$$

$$L_{right}^{3d} = 3.5 \times 10^{-10} H$$

$$L_{front}^{3d} = 9.7 \times 10^{-10} H$$

$l_{front} = 11.8mm$, $l_{left} = 12.7mm$ and $l_{right} = 12.7mm$.

Here the subscripts *left*, *right*, and *front* refer to the T-junction ports. C^{3d} and L^{3d} are the discontinuity capacitance and inductance.

The simulation is compared the results obtained with the full wave finite element simulator HFSS [7]. From HFSS, the propagation constant β on every port is 20.28

while from L^{2d} and C^{2d} , $\beta = \omega(L^{2d}C^{2d})^{\frac{1}{2}} = 20.47$. The calculated S-parameter from low frequency to 10GHz calculated by HFSS for this T-junction are given by the solid lines in Figure 6(b). The S-parameters obtained by using the discontinuity lumped elements of this paper for the junction calculated by using the microwave circuit simulator MDS [8] are given by the dashed lines in Figure 6(b). Good agreement is obtained up to 10GHz. Above 10GHz, a larger difference between the two simulations appears because full-wave effects become important.

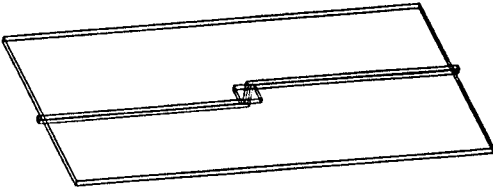


Figure 7: The geometry of a signal trace that goes through a ground plane.

4.3 Via and Ground Plane

Figure 7 shows a signal trace that goes under, then through, then above a ground plane. This example demonstrates the effect of the via on signal propagation. The calculated capacitance and inductance values for this model are

$$L_{front}^{2d} = 3.71 \times 10^{-7} H/m$$

$$C_{front}^{2d} = 2.93 \times 10^{-11} F/m$$

$$L^{3d} = 2.8 \times 10^{-9} H$$

$$C^{3d} = 4.79 \times 10^{-13} F$$

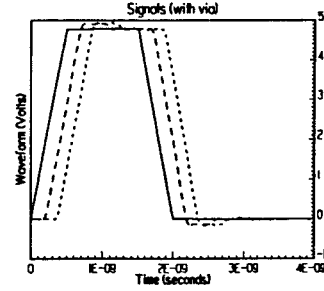
$$L_{back}^{2d} = L_{front}^{2d}, C_{front}^{2d} = C_{back}^{2d} \text{ and } l_{front} = l_{back} = 5cm.$$

Figure 8 shows the signals at both the near and far ends of the trace with and without the via discontinuity. The source and load are the same as in the previous examples. Due to the discontinuity at the via, distortion due to reflection at the discontinuity is observed in the signal.

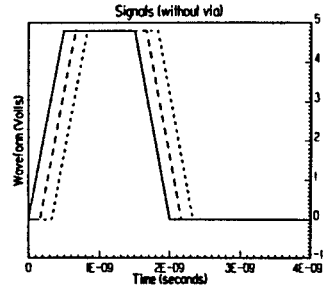
4.4 Cross-Talk on Multiple Lines

Figure 9 shows the structure of a three line interconnect which exhibits cross-talk. In this structure, the center line is grounded, the left line carries the active signal, and the right line is passive. The calculated capacitance and inductance matrices for this structure are

$$C_{front}^{2d} = \begin{bmatrix} 19.05 & -5.59 \\ -5.59 & 19.05 \end{bmatrix} pF/m$$



(a)



(b)

Figure 8: Signals at the near (solid line) and far (dotted line) ends, and at a point along the conductor (dashed line), (a) with and (b) without the via discontinuity.

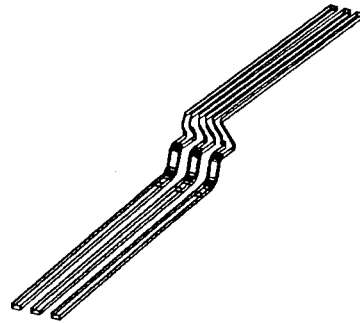


Figure 9: A three conductor interconnect exhibiting crosstalk.

$$C_{back}^{2d} = \begin{bmatrix} 20.49 & -5.93 \\ -5.93 & 23.68 \end{bmatrix} pF/m$$

$$L_{front}^{2d} = \begin{bmatrix} 6.37 & 1.89 \\ 1.89 & 6.37 \end{bmatrix} \times 10^{-7} H/m$$

$$L_{back}^{2d} = \begin{bmatrix} 5.85 & 1.47 \\ 1.47 & 5.06 \end{bmatrix} \times 10^{-7} H/m$$

$$C^{3d} = \begin{bmatrix} 0.103 & -0.033 \\ -0.033 & 0.11 \end{bmatrix} pF$$

$$L^{3d} = \begin{bmatrix} 5.66 & 1.77 \\ 1.77 & 4.08 \end{bmatrix} \times 10^{-9} H$$

$L_{front} = l_{back} = 0.39$ inch.

The near end of the active line is connected to an impulse voltage source and a 5 ohm source resistor. The far end of the active line and both ends of the passive line are terminated by 100 ohm resistors. Figure 10 shows the signals and crosstalk at both the near and far ends of the active and passive lines.

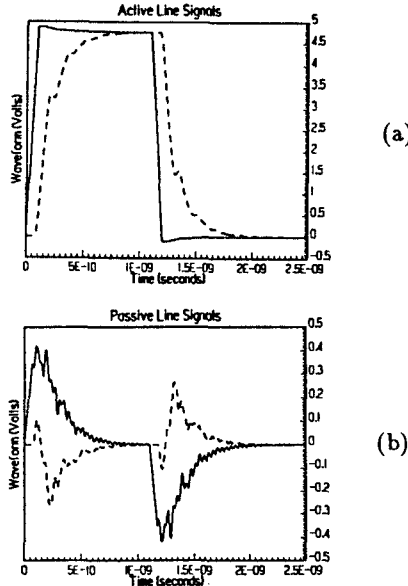


Figure 10: The signals at the near (solid line) and far (dashed line) ends of (a) the active line and (b) the passive line.

5 Conclusions

A technique for simulating high-speed digital interconnect circuits using the finite element method and SPICE has been developed. In this procedure, the electromagnetic fields in the interconnect are modeled as quasi-TEM waves. Multiconductor transmission lines are treated by using modal analysis while 3D discontinuities are represented by lumped capacitance and inductance matrices.

The accuracy of this approach depends on the accurate computation of 3D discontinuity inductance and capacitance matrices. In this paper, these matrices are computed by using the finite element method, defining ports and reference planes for the 3D regions. By requiring that 3D solutions on the ports be identical to the 2D port solutions, the traditional problem of overlap inductance and capacitance values is eliminated. Accurate 3D discontinuity inductance and capacitance matrices are then obtained by deembedding the port solutions back to the 3D discontinuity reference planes.

Comparisons of the simulated results with measurements and with a full-wave vector solutions in frequency domain show that for a typical circuit the method is accurate to 10GHz. The procedure is fully automated and the transient response of many interconnect circuits with pre-computed capacitance and inductance matrices takes only a few seconds. Best of all, the procedure is 100% SPICE compatible so that designers may simulate high-speed electromagnetic effects accurately within their existing SPICE environment.

Acknowledgment

We like to thank P. Premkumar, H. Maramis, S. Jan, H. Bhat, S. Gupta, A. Adel, D. Shenton, J. Gotow, M. Elliot, M. Knewston, A. Slavkovic and G. Kochaniak for contributing to this work. We also like to thank AMP, Inc. for the measurement data of the eight conductor example.

References

- [1] T Sarkar, Z. Maricevic, and M. Karhizi. An accurate de-embedding procedure for characterizing discontinuity. *Int. J. Micro- and Milli-meter Wave CAD*, 2(3):135, 1992.
- [2] T. Dhaene and D. De Dutter. Selection of lumped element models for coupled lossy transmission lines. 11(7):805, 1992.
- [3] T.Y. Chou and Z.J. Cendes. IC packages capacitance calculation using the finite element method. In *Proc. of Elect. Perform. of Elect. Packag. meeting*, 76, 1992.
- [4] Z.J. Cendes, D.N. Shenton, and H. Shahnasser. Magnetic field computation using delaunay triangulation and complementary finite element method. *IEEE Trans. on Magnetics*, 19(6):2551, 1983.
- [5] Z.J. Cendes and D.N. Shenton. Adaptive mesh refinement in the finite element computation of magnetic fields. *IEEE Trans. on Magnetics*, 21(6):1811, 1985.
- [6] F.Y. Chang. Computer-aided characterization of coupled tem transmission lines. *IEEE Trans on Circuit and Systems*, 27(12), 1980.
- [7] *High Frequency Structure Simulator (HFSS) User's Manual*. HP Corporation.
- [8] *Microwave Design System (MDS) User's Manual*. HP Corporation.